**Applied
Magnetic Resonance**

Time-Dependent Molecular Diffusion in Partially Filled Porous Glasses with Heterogeneous Structure

G. Farrher[1], **I. Ardelean**[2], and **R. Kimmich**[1]

[1] Sektion Kernresonanzspektroskopie, University of Ulm, Ulm, Germany
[2] Department of Physics, Technical University of Cluj-Napoca, Cluj-Napoca, Romania

Abstract. Nuclear magnetic resonance (NMR) microscopy of silica glasses with micrometer pores (Vitrapor#5) partially filled with water or cyclohexane reveals a heterogeneous distribution of liquid on a length scale much longer than the pore dimension. This heterogeneity, which is not observed in MR imaging of saturated samples, is attributed to the spatial variation of the granular microstructure visible in scanning electron micrographs. As a consequence of an inhomogeneous filling degree, the effective transverse relaxation time varies, which in turn leads to NMR imaging contrasts. Since the spatial distribution of the transverse relaxation time prevents reliable measurements with a standard pulsed gradient stimulated echo technique, a combination of the fringe field stimulated echo method, on the one hand, and the magnetization grid rotating-frame imaging technique, on the other, was employed. Four decades of the diffusion time from 100 ms to 1 s can be covered on this basis. The data were compared with Monte Carlo simulations of a model structure showing a qualitatively equivalent behavior in the common time window. The self-diffusion in partially filled porous systems is known to be strongly affected by a vapor phase. Here we have shown that the vapor phase contribution to the effective diffusivity is particularly efficient on a diffusion time scale corresponding to mean-squares displacements of the order of the pore dimension.

1 Introduction

Porous silica glasses are random objects intrinsically implying spatially fluctuating heterogeneities of the local pore size, the local magnetic susceptibility, the local transverse relaxation time of fluid, the local diffusion coefficient and other properties. These heterogeneities can be characterized by introducing spatial correlation functions defined as $\left\langle f\left(\vec{r}_0\right) f\left(\vec{r}_0 + \vec{r}\right)\right\rangle$, where $f\left(\vec{r}\right)$ is a property of the porous medium at the position $\vec{r}$. The function $f\left(\vec{r}\right)$ can be the fluctuating part of any of the quantities mentioned above. Assuming a vanishing ensemble average for spatial fluctuations, that is, $\left\langle f\left(\vec{r}\right)\right\rangle = 0$, and the coarse grain isotropy, we can restrict ourselves to an arbitrary direction, for example, x. The correlation length l_c of any of those quantities is then defined by

$$l_c \equiv \int\limits_0^\infty \frac{\langle f(x_0)f(x_0+x)\rangle}{\langle f^2(x_0)\rangle}\, \mathrm{d}x.$$

If the spatial correlation function is monoexponential, this definition is consistent with $\langle f(x_0)f(x_0+x)\rangle\big/\langle f^2(x_0)\rangle = \exp(-x/l_c)$.

The correlation length may vary in an extremely wide range depending on the material. It will be shown that the porous glass mainly studied in the present paper, Vitrapor#5, with a nominal pore size of about 1 µm is subjected to heterogeneities almost approaching the sample size. One may speculate that the correlation length characterizing the extension of spatial fluctuations scales with the nominal pore size. That is, porous glasses such as the well-known and frequently studied Vycor with a nominal pore size of 4 nm may be subjected to the same sort of heterogeneities, which, however, are scaled down to a correlation length below the spatial resolution of magnetic resonance (MR) microscopy.

The use of a porous glass with pores in the micrometer regime thus permits to explore the nature of heterogeneities and their influence on measuring quantities such as the diffusion coefficient. The spatial variation of the fluid properties thus can readily be studied in the frame of the spatial resolution of MR microscopy [1, 2]. It is the objective of the present study to demonstrate the material heterogeneities relevant for nuclear magnetic resonance (NMR) parameters and to compare them with scanning electron microscopy (SEM) images as far as available for systems with different nominal pore size and preparation history.

Unsaturated porous media are systems of coexisting liquid and vapor phases subjected to geometrical restrictions by the pore network, molecular exchange, and adsorption–desorption processes. The consequence is that the effective diffusion coefficient tends to be a function of the diffusion time t. A time-dependent diffusion coefficient is defined by

$$D(t) = \langle r^2(t)\rangle\big/6t, \tag{1}$$

where $\langle r^2(t)\rangle$ is the mean-squares displacement of molecules. The time dependence is of particular interest since it globally reflects the spatial distribution of liquid in the pore space, the molecular exchange rates, the polarity of liquid and pore walls, and the geometrical character of the confining pore space.

Apart from treatment of the model unspecific limits of time-dependent diffusion coefficients [3–5] and scaling arguments for certain percolation and fractal models [6], first-principles theoretical descriptions of the diffusion in partially filled pore spaces are rare. The reason is the complex nature of the microstructure that cannot be expressed in simple terms. Monte Carlo simulations are, therefore, a good way to relate and compare the experimental data with the model treatments.

There are a number of models for the spatial fluid distribution in partially filled porous media [7, 8]. These morphology models often refer to the structure units such as plugs, puddles, surface layers of constant thickness, etc., which seem to be of a somewhat artificial character. In the present study, we therefore try to

model the spatial distribution of fluid in a more natural way: by assuming a granular type of the porous matrix (as it occurs in typical porous silica glasses) and considering more or less overlapping liquid surface layers, the structure elements, such as plugs, interface layers of varying thickness, and dropletlike accumulations of the liquid phase, are produced automatically. Monte Carlo simulations of the molecular diffusion in this sort of a model system will be the main tools for the interpretation of the experimental NMR results.

2 Sample Preparation and Characterization

2.1 Samples and Filling Fluids

Three different porous samples were investigated: two commercial silica glasses and a bimodal system (sample III). Two different silica glasses with pores in the mesoscopic range are Vitrapor#5 (nominal pore size, 1 ± 0.6 μm; porosity, 0.43) and Vycor (nominal pore size, 4 ± 0.6 nm; porosity, 0.28). Vitrapor#5 was purchased from ROBU Glasfilter-Geräte GmbH, Germany. Vycor VPQ#7930 was purchased from Corning Ltd. The samples were pretreated as suggested by the manufacturer. This includes 30 min boiling in 30% H_2O_2. The samples were then washed with distilled water and left in vacuum for 24 h at 95 °C. After that, the samples were considered to be dry. That is, the nominal filling factor f was set to zero under such conditions.

The third system (sample III) was prepared in the Department of Inorganic Chemistry of Ulm University and was only used as a reference for comparison. As will be shown below, this system does not show the heterogeneities characteristic for silica glasses with a granular microstructure. Sample III had a bimodal pore size distribution with peaks at about 10 and 0.6 mm.

The adsorbate fluids, water and cyclohexane, were chosen as typical representatives of polar and nonpolar species. The water was demineralized. N-Cyclohexane was purchased from Fluka Chemika, Germany. The fluids were filled into the porous glass either via adsorption (the dry material was placed into a saturated atmosphere until the desired filling factor was reached) or via desorption (the saturated material was exposed to a dry atmosphere until the desired degree of filling was established). In either case the filling factor was determined by weighting. In the adsorption mode (AM), the adsorbate was heated to 60 °C in order to increase the vapor pressure and hence to accelerate the uptake of the adsorbate in a porous material. In the desorption mode (DM), the sample was first saturated by the bulk-to-bulk method resulting in a filling factor of 1. Afterwards the liquid in pores was partially evaporated by putting the sample in a glove bag with a dry nitrogen atmosphere. In this way, any contact with the air humidity was avoided. After preparation, the samples were sealed in a sample container with practically no empty space for further evaporation. The extended annealing of the samples did not perceptibly affect the heterogeneous distribution of liquid in the samples (see below).

2.2 Heterogeneities

NMR micrographs were recorded by the standard three- or two-dimensional (2-D) Fourier-transform (FT) imaging techniques, which are based on Hahn echo pulse sequences (see refs. 1 and 2 for details). Cross-sectional images are rendered in Figs. 1 and 2. All parameters of the sample preparation and image acquisition are given in the legends or specified directly in the images. The experiments were performed at 20 °C on a Bruker DSX 400 MHz NMR spectrometer equipped with a microscopy gradient unit. The maximum strength of gradient pulses obtained with this instrument both for imaging and diffusometry was 1 T/m.

Figure 1a shows a cross-sectional NMR image of a Vitrapor#5 sample saturated with water ($f = 1$). Apart from noise, no contrast inside the sample can be identified. That is, the voxel-average water spin density and the voxel-average transverse and longitudinal relaxation times do not vary from voxel to voxel with the voxel dimension being much larger than the nominal pore size.

The situation in unsaturated samples is quite different for both water (polar) and cyclohexane (nonpolar). Figure 1b and c shows cross-sectional NMR micrographs of Vitrapor#5 samples with a filling degree $f = 0.6$ for water and cyclohexane, respectively. Obviously there are light spots indicating a high content of the liquid phase irrespective of the polarity of the adsorbate liquid. The spatial distributions are almost identical for both liquids.

The samples in Fig. 1b and c were prepared in the DM. The way the samples are filled appears to have relatively little influence on the spatial distribution as demonstrated in Fig. 1d and e for the case of water in Vitrapor#5. Irrespective of whether the DM or AM was used, the heterogeneous distribution of the liquid phase turns out to be rather similar.

One might think of a metastable distribution of the liquid phase fortuitously arising due to some imponderabilities in the preparation procedure. However, even extended annealing periods (up to weeks) of the sealed samples at elevated temperatures (up to 90 °C) did not change the coarse grain distribution of the liquid phase (compare Fig. 1f and d). It appears that the spatial distribution does not depend on the preparation history. It can also be not solely due to the instability between the vapor and liquid phases as a consequence of the competition between the cohesion and adhesion forces. This would stipulate much more variability in the morphology of the spatial phase distribution than the observed one. The conclusion is that the heterogeneity is of a microstructural origin.

Actually SEM micrographs suggest this sort of heterogeneity. Figure 2a and b indicates not only the granular nature of Vitrapor#5 but also some variation in the porosity, grain and pore size. The two micrographs have been taken from light (Fig. 2a) and dark (Fig. 2b) areas, so that the different microstructure visible in SEM appears to correlate with the contrasts in the NMR images. This observation was made coincidently for several parts of the sample.

In Fig. 1 the NMR images are strongly weighed by relaxation. In particular, liquid in the light spots tends to have a T_2 longer than that in the darker areas. An explanation is that the higher filling degree in the light spots produces a more homogeneous filling and, hence, less susceptibility fluctuations.
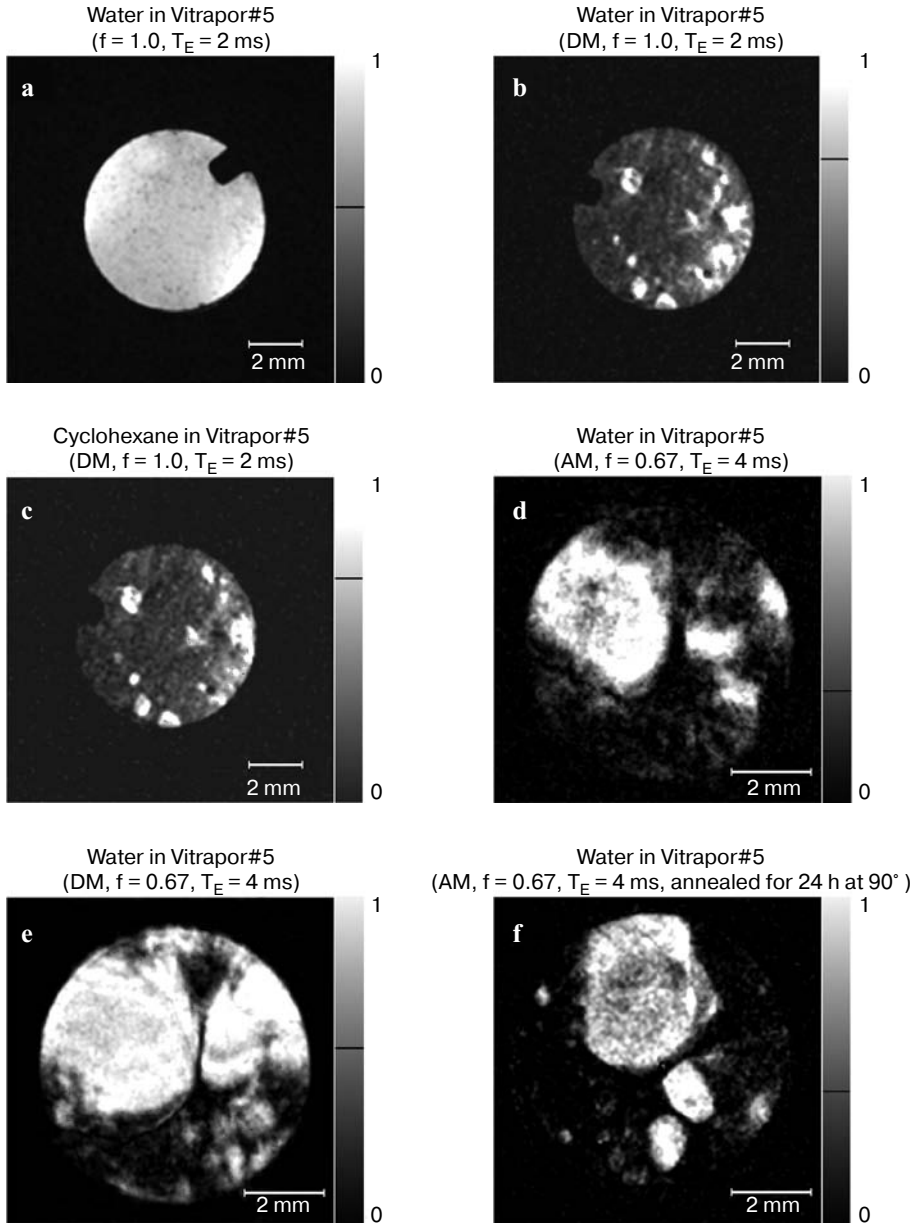
Water in Vitrapor#5
($f = 1.0$, $T_E = 2$ ms)

Water in Vitrapor#5
(DM, $f = 1.0$, $T_E = 2$ ms)

Cyclohexane in Vitrapor#5
(DM, $f = 1.0$, $T_E = 2$ ms)

Water in Vitrapor#5
(AM, $f = 0.67$, $T_E = 4$ ms)

Water in Vitrapor#5
(DM, $f = 0.67$, $T_E = 4$ ms)

Water in Vitrapor#5
(AM, $f = 0.67$, $T_E = 4$ ms, annealed for 24 h at 90°)

Fig. 1. NMR micrographs of saturated and unsaturated porous silica systems. The proton signals refer to fluid. The echo time (T_E), the filling factor (f) and the preparation method (DM, AM) are indicated in the images. The repetition time T_R was 1 s in all cases. The cross sections are either directly measured using a 2-D slice selective imaging sequence (2-D FT; slice width, 1 mm) or were evaluated from 3-D data sets acquired in 3-D imaging experiments (3-D FT; slice width equals the digital resolution). The field of view (FOV) was 8 or 12 mm, the digital resolution (DR) was 62 or 94 μm. **a** and **b** Water in Vitrapor#5: 3-D FT; FOV, 12 mm; DR, 94 μm. **c** Cyclohexane in Vitrapor#5: 3-D FT; FOV, 12 mm; DR, 94 μm. **d–f** Water in Vitrapor#5: 2-D FT; FOV, 8 mm; DR, 62 μm.
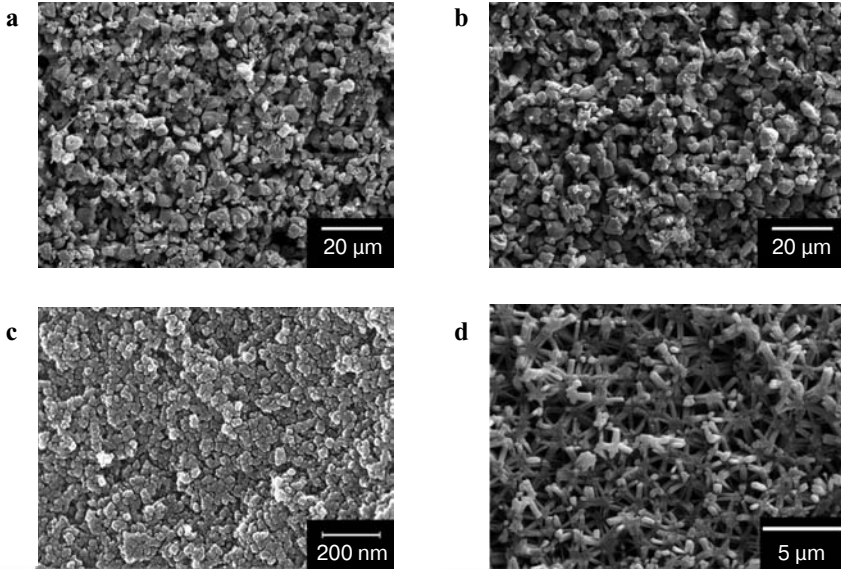
Fig. 2. **a** and **b** SEM images of Vitrapor#5 (1.0 µm pore size), **c** Vycor (4 nm pore size), **d** bimodal silica system (sample III). The granular character of the Vitrapor#5 and Vycor samples is obvious. **a** and **b** Images from the areas appearing as light and dark in the NMR image of Vitrapor#5 shown in Fig. 1d, respectively. No differences could be observed in the micrograph taken from different areas both in the case of Vycor and the bimodal silica system (sample III).

The Vitrapor#5 samples are specified by a nominal pore size of 1.0–1.6 mm. That is almost three orders of magnitude greater than the pores in Vycor. NMR images of unsaturated Vycor (Fig. 3a and b) consequently do not show the heterogeneities observed with Vitrapor#5. The only contrasts that can be identified are due to noise and surface tension phenomenon leading to a corona which arises in the DM (Fig. 3b).

On the other hand, the microstructure of Vycor, as far as visible in SEM, looks very similar to that of Vitrapor#5. Figure 2c shows again the granular type of the structure already known for Vitrapor#5. The main difference appears to be the length scale of the grain size. Hence, the correlation length of Vycor is far below the spatial resolution of any NMR image.

It is often assumed that the correlation length of a porous medium is of the order of a few pore diameters. However, the fact that it is possible to visualize the microscopic heterogeneities in the structure of the Vitrapor#5 sample partially filled with liquids indicates much longer correlation lengths.

Figure 3c shows an NMR image of another partially filled material (sample III) for comparison. A representative SEM micrograph of this sample is shown in Fig. 2d. This sample was prepared in the Department of Inorganic Chemistry of Ulm University and is again a porous silica system but with a bimodal pore structure. The pore dimensions are nanometers, on the one hand, and micrometers, on the other. The latter pore type dominates. Most important with this sample
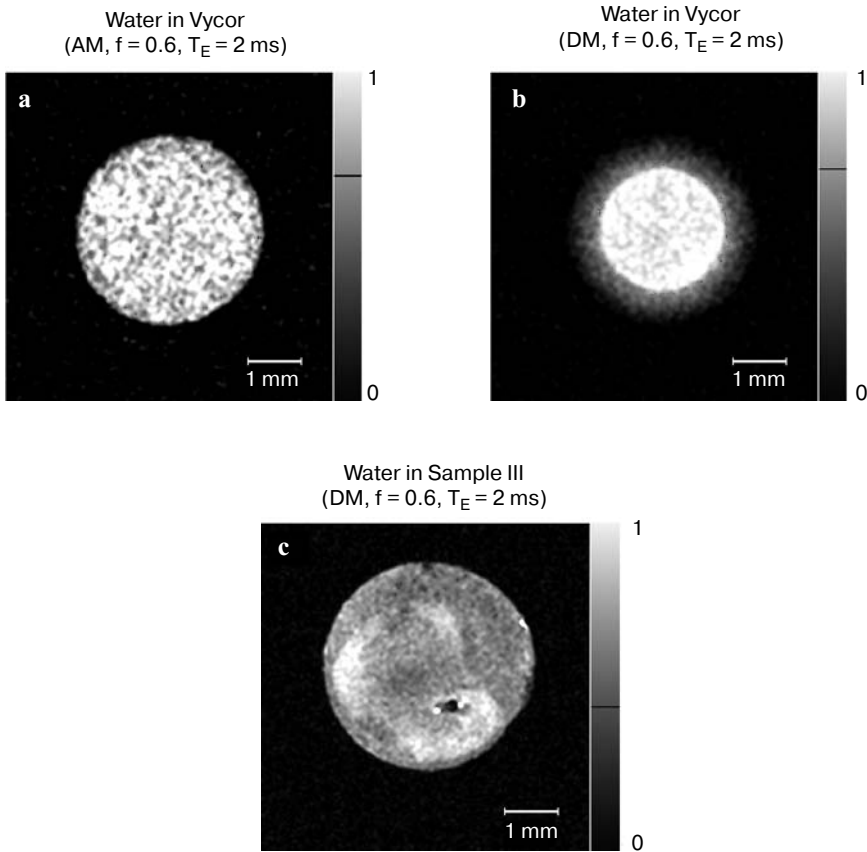
Water in Vycor
(AM, f = 0.6, T_E = 2 ms)

Water in Vycor
(DM, f = 0.6, T_E = 2 ms)

Water in Sample III
(DM, f = 0.6, T_E = 2 ms)

Fig. 3. Same as in Fig. 1 but water in Vycor: 3-D FT; FOV, 6 mm; DR, 47 μm (**a** and **b**); and water in a bimodal silica system (sample III): 3-D FT; FOV, 6 mm; DR, 47 μm (**c**).

is that it is not of the granular type visible in the SEM micrographs shown in Fig. 2a–c. The NMR image and the SEM micrographs suggest an essentially homogeneous structure with a correspondingly short correlation length below the image resolution. That is, the correlation length is not determined by the pore size only. The granular nature of the other two systems is also relevant.

3 Effect of Heterogeneity on Diffusion Measurements

3.1 Diffusion Techniques

In order to perform reliable time-dependent difussion studies in partially filled porous samples the choice of an appropriate technique is essential. Apart from the standard pulsed gradient spin echo technique [9], there are other NMR diffusometry methods of interest for porous materials [10]. Since we are interested in

the time dependence of the diffusion coefficient, the techniques should be particularly flexible in this respect. Another important condition is the insensitivity to internal gradients and distributions of the local transverse relaxation time T_2.

As suggested in a previous study [11], a particularly favorable combination of NMR diffusometry methods is the fringe field stimulated echo (FFStE) technique [12–14] for relatively short diffusion times (100 μs $< t <$ 10 ms), and the magnetization grid rotating-frame imaging (MAGROFI) variant [11, 15, 16] for long diffusion times (10 ms $< t <$ 1 s). The former is insensitive to internal gradients due to the large external field gradient employed (up to 60 T/m on our spectrometer), the latter because of the use of gradients of the radio frequency (RF) amplitude, which is practically not affected by inhomogeneities of the magnetic susceptibility. Owing to the extremely short coherence evolution intervals of the FFStE method and the fact that the MAGROFI technique is essentially based on the evolution of the longitudinal magnetization, the transverse relaxation, in general, and distributions of the local T_2, in particular, are of negligible influence.

Figure 4 shows the pulse schemes for the NMR diffusometry experiments in this study. The FFStE pulse sequence (Fig. 4a) consists of three RF pulses. The spin coherences evolve in the presence of the steady external gradient G of the fringe field of a superconducting magnet. For the present experiments, the field gradient was chosen to be $G = 22$ T/m at a position of 15.6 cm below the center of the magnet. The probe for the FFStE experiments was tuned to 375 MHz at a field gradient of 22 T/m. The magnetic flux density and its gradient were first crudely measured using a homebuilt Hall probe. The gradient was then calibrated with the known diffusion coefficient of bulk water.

The attenuation factor of the stimulated echo following the third RF pulse is given by [2]

$$A = A_0 \exp\left(-D\gamma^2 G^2 \tau_1^2 \left([2/3]\tau_1 + \tau_2\right)\right)\exp\left(-\frac{2\tau_1}{T_2}\right)\exp\left(-\frac{\tau_2}{T_1}\right),$$

where D is the diffusion coefficient, γ is a gyromagnetic ratio and T_1 and T_2 are the longitudinal and transverse relaxation times, respectively. Note that the diffusive displacements during the interval τ_1 (see Fig. 4a) can be neglected as long as the condition $\tau_1 \ll \tau_2$ is fulfilled, so that the diffusion time can be equated with τ_2. On the other hand, if the τ_2 interval is comparable with τ_1, the diffusion time can be defined by $t_{\text{diff}} \equiv (2/3)\tau_1 + \tau_2$, which is to be kept constant in an experiment [11].

The time interval τ_1 was varied from 10 to 106 μs in 32 steps. Due to the fringe field gradient, T_2^* was extremely short (approximately 1.2 μs). That is, diffusion times as short as 100 μs can be easily reached and the FFStE diffusion time window covers the range from 100 μs to 10 ms. The influence of the transverse and longitudinal relaxation was eliminated by repeating exactly the same pulse experiment in a homogeneous field of practically the same strength. The division of the stimulated echo amplitudes with and without field gradient then
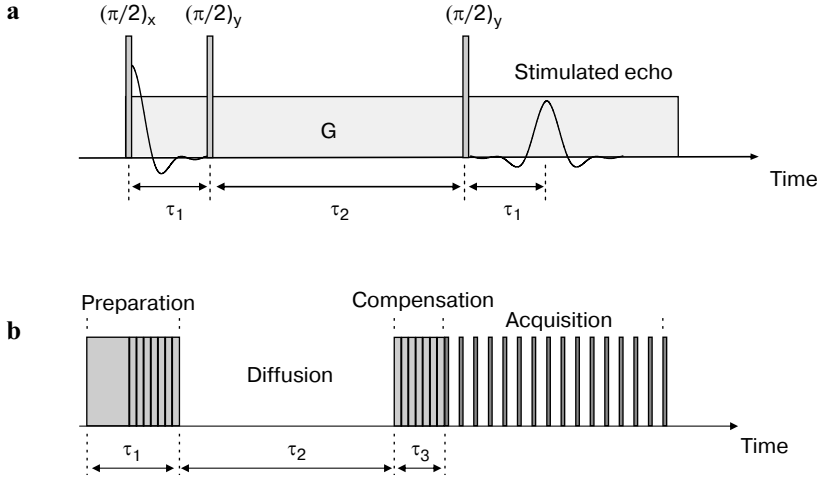
Fig. 4. a Schematic representation of the RF pulses and the steady field gradient for the FFStE variant of NMR diffusometry. In the present study, a steady gradient $G = 22$ T/m is applied along the z-axis. The time τ_1 is varied from 10 to 106 µs in 32 steps. **b** RF gradient pulse scheme of the MAGROFI experiment as used in the present study. The preparation pulse is incremented in subsequent transients from a starting value of 180 µs in 32 steps of $\tau_R = 20$ µs each. The magnetization grid produced by the preparation pulse is recorded after the diffusing interval by a rapid rotating-frame imaging technique. The compensation pulse effectively stretches the magnetization grid to be imaged so that the wavelength of the modulation remains independent of the preparation pulse length.

provides the echo attenuation factor due to the diffusion alone. Alternatively, self-compensating pulse sequences can be employed as reported in refs. 12–14.

The principle of the MAGROFI method is schematically shown in Fig. 4b. The technique is based on gradients of the RF amplitude [17]. In order to produce favorable B_1 gradients for the MAGROFI experiments, the RF coil of an ordinary probe head of the system was replaced by a conic coil [11], which was used both for excitation and detection.

In the preparation interval, a magnetization grid (or grating) is prepared. A diffusion interval follows. After compensation of the evolution due to the increments of the preparation interval, the longitudinal magnetization distribution is imaged by a rapid rotating-frame imaging technique.

The width of the preparation and compensation pulses was synchronously incremented in 32 steps of 30 µs each. The initial duration of the preparation pulse was 180 µs. After the interval τ_3 (see Fig. 4b), 1-D rapid rotating-frame images were rendered by acquiring the pseudo free induction decay (FID) with a train of 200 pulses, each 2 µs long followed by stroboscopic acquisition of the signals between the pulses. The FT of this pseudo FID provides an image of the z-magnetization that is attenuated by relaxation and diffusion phenomena. The diffusion coefficient is evaluated according to [11]

$$A(x, \tau_1) = A_0 \cos\left[\gamma B_1(x)\tau_1\right] \exp\left(-D\left[\gamma G_1(x)\right]^2 \tau_1^2 \tau_2\right) \exp\left(-\frac{\tau_2}{T_1}\right). \qquad (2)$$

Here $B_1(x)$ is the local amplitude of the RF field and $G_1(x) = \partial B_1(x)/\partial x$ is the corresponding gradient. These quantities were evaluated as described in ref. 11. In Eq. (2), the diffusive displacements during the preparation and imaging intervals (see Fig. 4b) have been neglected. Otherwise, the formalism analogous to the Stejskal–Tanner treatment [9] for finite field gradient pulses must be employed. In the case of our samples, the total time window accessible by the MAGROFI technique ranges from 10 ms to 1 s. Note that Eq. (2) does not depend on the transverse relaxation time T_2. That is, MAGROFI diffusometry is not only insensitive to the internal field gradients but also to the transverse relaxation. More detailed descriptions and discussions can be found in refs. 11, 15 and 16.

3.2 Heterogeneity Effects

The transverse relaxation in unsaturated porous glasses is expected to be largely inhomogeneous as a consequence of the spatially varying filling degree. Anticipating that the relaxation rates are weighed by the fraction of molecules in the adsorption layer at the solid-to-liquid interfaces, one concludes that a locally large filling degree leads to long relaxation times, whereas the surfaces just covered by a thin liquid layer with no surrounding bulklike water will produce short relaxation times. Both situations occur in partially filled pore spaces. Any NMR technique for measuring diffusion coefficients should therefore be particularly insensitive to spatial variations of the transverse relaxation time T_2. Figure 5 shows data for water in unsaturated Vitrapor#5 measured with the pulsed gradient stimulated echo (PGStE) and MAGROFI techniques as a function of the encoding time τ_1.

The PGStE data increase with decreasing τ_1, which indicates the increasing signal contribution of short T_2 phases. The extrapolation of the PGStE data to the limit $\tau_1 \rightarrow 0$ approaches the value measured with the MAGROFI technique, which is practically insensitive to the transverse relaxation.

The MAGROFI data, in turn, coincide with those measured with the FFStE method in the overlap regime of diffusion times [11]. The conclusion is that the FFStE technique combined with MAGROFI renders the effective diffusion coefficient averaged over the whole sample irrespective of the local T_2 in the whole time range of these two techniques. This is in contrast to the PGStE measurements which range predominantly refer to the light (i.e., long T_2, high filling factor) spots visible in the NMR micrographs of Fig. 1 in the accessible τ_1 (see also the dependence of the diffusion coefficient on the filling factor reported in ref. 18).

Similar deviations were found also for the diffusion coefficient of water in partially filled Vycor measured with MAGROFI or PGStE techniques. For a given filling factor, the diffusion coefficients become higher when using the MAGROFI technique. This could be an indication that the Vycor sample has also a heteroge-
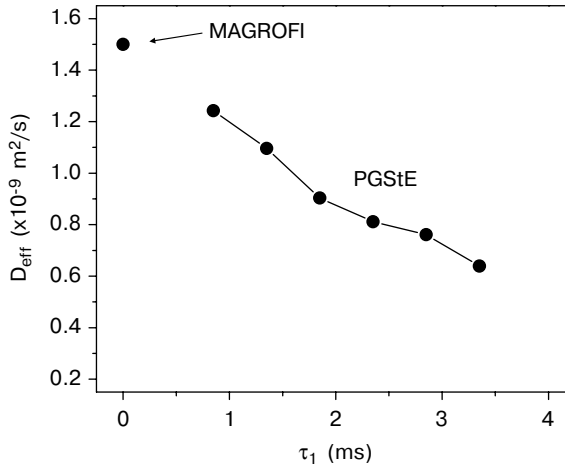
Fig. 5. Effective diffusion coefficient of water in unsaturated Vitrapor#5 measured with the PGStE technique for different encoding times. The filling factor was $f = 0.5$. Extrapolation to the limit $\tau_1 \rightarrow 0$ approaches the diffusion coefficient measured with the MAGROFI technique. This demonstrates the sensitivity of the PGStE method to the spatial distributions of the transverse relaxation time, whereas MAGROFI practically does not depend on T_2.

neous distribution of liquid but undetectable in our MR microimages. On the contrary, when the sample III was partially filled with water, the diffusion coefficients measured with MAGROFI and PGStE techniques were found to be the same. This is in agreement with the homogeneous liquid distribution observed in Fig. 3c.

4 Time-Dependent Diffusion Studies

4.1 Experimental Results

Due to the influence of heterogeneity described above, the time-dependent diffusion measurements were performed using FFStE and MAGROFI techniques. The effective water diffusion coefficient was measured in Vitrapor#5 with different filling factors. The data are for the diffusion times between 100 µs and 1 s plotted in Fig. 6a. As far as investigated in this study, the values decrease with increasing filling factor as a consequence of the decreasing vapor-phase contribution [19–26]. The time dependence of the diffusion coefficient of water in partially filled porous glass also reflects the obstruction by the pore space tortuosity.

4.2 Monte Carlo Simulations

In order to understand the experimental data, Monte Carlo simulations of the translational diffusion were performed for 2-D model pore spaces (Fig. 7). Up to 100 million molecular steps with a length corresponding to 1 and 100 nm in the liq-
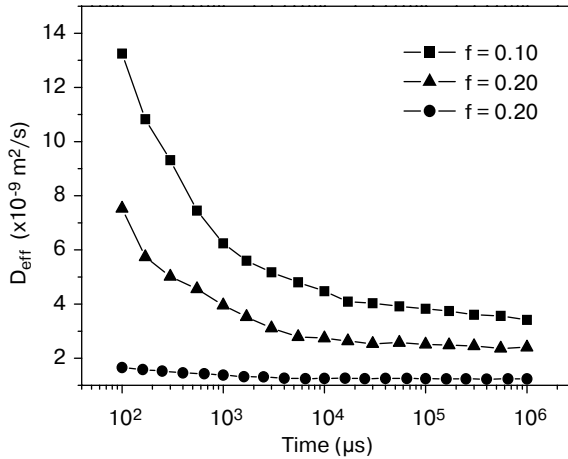
Fig. 6. Effective (overall average) diffusion coefficient versus the diffusion time for different filling factors. The data were measured by a combination of FFStE and MAGROFI techniques.

uid and vapor phases, respectively, were simulated using the random number generator routine ran3 described in ref. 27. The difference of two orders of magnitude in the step length between the two phases corresponds to the four-order higher diffusion coefficients known for gases relative to liquids.

The number of fluid molecules considered in the simulation was varied for different diffusion times. For very short times beginning with 125 ps, ten million particles were necessary to obtain the same statistical accuracy as for long times up to 12.5 ms, where only thousand particles were sufficient.

The 2-D pore space is defined in a plane with orthogonal Cartesian coordinate axes x and y. For each molecular step, two numbers x and y are randomly generated between -1 and $+1$. The step coordinates are then calculated as
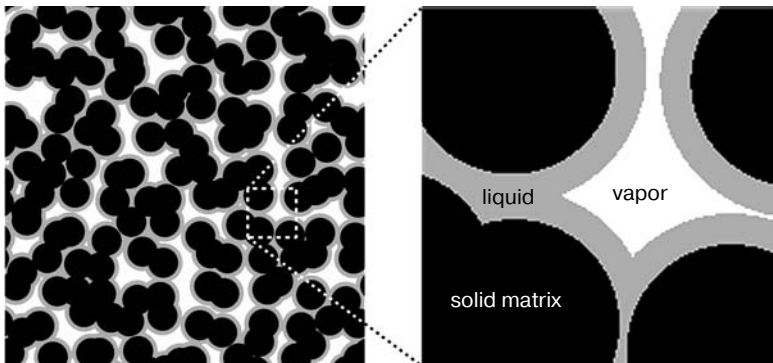

Fig. 7. Spherical-grain pack structure the Monte Carlo simulations refer to. The solid grains are represented in black, the liquid phase in gray, and the vapor phase in white.

$$\Delta x = \frac{x}{\sqrt{x^2 + y^2}}, \quad \Delta y = \frac{y}{\sqrt{x^2 + y^2}}.$$

The step is cancelled if it leaves the predefined pore space. The mean-squares displacement starting from a randomly chosen initial position was determined as a function of time, and the time-dependent diffusion coefficient was evaluated according to Eq. (1).

Since the density of the liquid phase is three orders of magnitude higher than that in the vapor phase, practically the whole signal detectable in our NMR experiments originates from the liquid phase. It is therefore sufficient to consider merely those molecules in the simulations that currently reside in the liquid phase (but perhaps have been subjected to displacements in the vapor-phase areas before).

The Monte Carlo simulations were performed for a grain pack structure as shown in Fig. 7. For the 2-D case, the solid grains are represented by circular, partially overlapping discs. The diameter of these circular discs corresponds to 1 µm. The discs were placed at random distances from the points of a square lattice with a unit cell dimension of 1 µm. The distance vectors from the lattice points to the associated discs were varied randomly with respect to the direction and magnitude. The magnitude varied in the range of 0–0.4 µm. The mean pore size resulting in this way is 0.97 µm.

The disc surfaces as far as facing the pore space were assumed to be covered with a liquid layer of constant thickness (see Fig. 7). The remaining pore
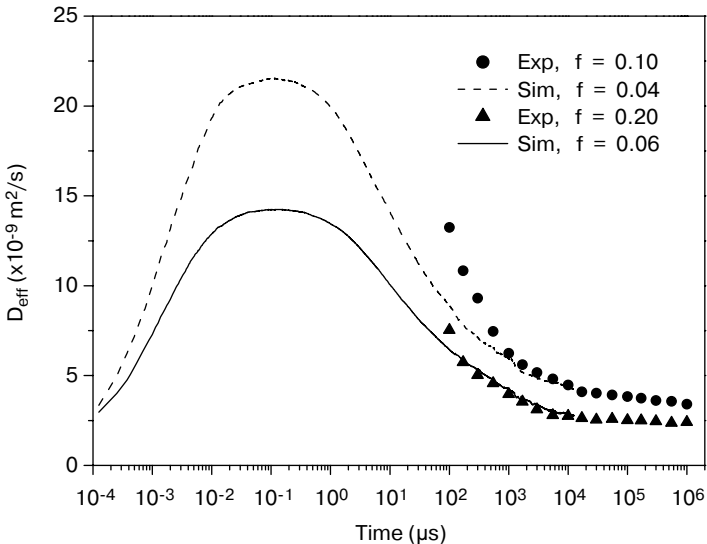

Fig. 8. Effective (overall average) diffusion coefficient as a function of time for filling factors $f = 0.1$ and $f = 0.2$. The experimental data (circles and triangles) are compared with the results of the Monte Carlo simulations (solid and broken curves).

space represents the vapor phase. When a particle reaches the liquid-to-vapor interface, its probability per unit time (step time) to escape from the liquid phase to the vapor phase was assumed to be $P_{l \to v} = 0.01$. Likewise the probability per unit time that a particle enters liquid coming from the vapor phase was taken as $P_{v \to l} = 0.99$. As a third exchange mechanism, the adsorption and desorption at the solid-matrix walls were considered. The corresponding probabilities per unit time were assumed to be $P_{ads} = 0.9$ and $P_{des} = 0.1$, respectively.

Figure 8 shows the results of Monte Carlo simulations based on the 2-D grain model structure rendered in Fig. 7 in the case of two filling factors ($f = 0.04$ and $f = 0.06$). As can be observed, the simulations reproduce the qualitative tendency of the time dependence in the same experimental time window. This means that the essential features of the pore space-restricted diffusion are accounted for. However, the absolute values are significantly different. The reason for the quantitative discrepancies must be sought in the simplicity of the 2-D model structure in Fig. 7. In particular, the model does not take into account the heterogeneities detected in the microscopy experiments.

5 Conclusions

The first finding of our work is related to the correlation length of a porous media. It is often assumed that the correlation length is of the order of a few pore diameters. Here, it was possible to visualize the microscopic heterogeneities in the structure of the Vitrapor#5 sample partially filled with liquid. These images serve as an indication for much longer correlation lengths. The contrast in the NMR microimages exaggerates the real, practically relevant heterogeneity of the samples as can also be concluded from the SEM micrographs. The NMR image contrasts are largely dominated by T_2 which strongly varies across the Vitrapor#5 samples. This, however, does not exclude the lower heterogeneous distributions of the filling factor and the local effective diffusion coefficient.

The second finding is that in systems with heterogeneities it is essential to use NMR diffusometry methods insensitive to the spatial T_2 distributions. The techniques employed here (FFStE and MAGROFI) proved to be particularly suitable, while the standard PGStE method is not appropriate for the sample conditions of this study. That is why the methods that are employed for our time-dependent diffusion studies in partially filled porous media are FFStE and MAGROFI. These two techniques provide effective diffusion coefficients not affected by the spatial variations of the transverse relaxation time.

Another finding is that the diffusion coefficients of liquids in partially filled porous glasses are close to their bulk values in the short time limit corresponding to few molecular diffusion steps. When the mean-squares displacement approaches the mean pore size, a maximum is reached, indicating a significant contribution of the vapor phase to the effective diffusion coefficient via exchange between the two phases (liquid and vapor). Under present conditions, the maximum value is more than one decade larger than the diffusion coefficient in the bulk liquid. At longer diffusion times (or mean-squares displacement), the ob-

struction by the tortuosity of the pore space occurs. The effective diffusion co-efficient decays until a reduced effective value close to the bulk liquid value is reached on a length scale beyond the correlation length. The experimental data are well reproduced in the common time window by Monte Carlo simulations on a model structure.

Acknowledgments

References

1. Blümich, B.: NMR Imaging of Materials. Clarendon, Oxford (2000)
2. Kimmich, R.: NMR: Tomography, Diffusometry, Relaxometry. Springer, Berlin (1997)
3. Mitra, P.P., Sen, P.N., Schwartz, L.M., Le Doussal, P.: Phys. Rev. Lett. **68**, 3555 (1992)
4. Mitra, P.P., Sen, P.N., Schwartz, L.M.: Phys. Rev. B **47**, 8565 (1993)
5. Latour, L.L., Mitra, P.P., Kleinberg, R.L., Sotak, C.H.: J. Magn. Reson. A **101**, 342 (1993)
6. Orbach, R.: Science **231**, 814 (1986)
7. Valiullin, R., Skirda, V., Stapf, S., Kimmich, R.: Phys. Rev. E **55**, 2664 (1997)
8. Allen, S.G., Stephenson, P.C.L., Strange, J.H.: J. Chem. Phys. **106**, 7802 (1997)
9. Stejskal, E.O., Tanner, J.E.: J. Chem. Phys. **42**, 288 (1965)
10. Ardelean, I., Kimmich, R.: Annu. Rep. Nucl. Magn. Reson. Spectrosc. **49**, 43 (2003)
11. Farrher, G., Ardelean, I., Kimmich, R.: J. Magn. Reson. **182**, 215 (2006)
12. Kimmich, R., Fischer, E.: J. Magn. Reson. A **106**, 229 (1994)
13. Fischer, E., Kimmich, R.: J. Magn. Reson. **166**, 273 (2004)
14. Demco, D.E., Johansson, A., Tegenfeldt, J.: J. Magn. Reson. A **110**, 183 (1994)
15. Kimmich, R., Simon, B., Köstler, H.: J. Magn. Reson. **112**, 7 (1995)
16. Simon, B., Kimmich, R., Köstler, H.: J. Magn. Reson. A **118**, 78 (1996)
17. Canet, D.: Prog. Nucl. Magn. Reson. Spectrosc. **30**, 101 (1997)
18. Farrher, G., Ardelean, I., Kimmich, R.: Magn. Reson. Imaging **25**, 453 (2007)
19. Ardelean, I., Farrher, G., Mattea, C., Kimmich, R.: J. Chem. Phys. **120**, 9809 (2004)
20. Kärger, J., Pfeifer, H., Riedel, E., Winkler, H.: J. Colloid Interface Sci. **44**, 187 (1973)
21. D'Orazio, F., Bhattacharja, S., Halperin, W.P., Gerhardt, R.: Phys. Rev. Lett. **63**, 43 (1989)
22. Kimmich, R., Stapf, S., Callaghan, P., Coy, A.: Magn. Reson. Imaging **12**, 339 (1994)
23. Kimmich, R., Stapf, S., Seitter, R.O., Callaghan, P., Khozina, E.: Mater. Res. Soc. Symp. Proc. **366**, 189 (1995)
24. Valiullin, R., Naumov, S., Galvosas, P., Kärger, J., Woo, H.-J., Porcheron, F., Monson, P.A.: Nature **443**, 965 (2006)
25. Valiullin, R., Kortunov, P., Kärger, J., Timoshenko, V.: J. Chem. Phys. **120**, 11804 (2004)
26. Ardelean, I., Mattea, C., Farrher, G., Wonorahardjo, S., Kimmich, R.: J. Chem. Phys. **119**, 10358 (2003)
27. Press, W.H., Flannery, B.P., Teukolsky, S.A., Vetterling, W.T.: Numerical Recipes in C. Cambridge University Press, Cambridge (1990)

Authors' address: Ioan Ardelean, Department of Physics, Technical University of Cluj-Napoca, Cluj-Napoca 400020, Romania
E-mail: ioan.ardelean@phys.utcluj.ro